Chinese Journal of
POLYMER SCIENCE

RESEARCH ARTICLE

https://doi.org/10.1007/s10118-026-3648-z
Chinese J. Polym. Sci.

Interlaminar Shear Strength Parameter, Durability Change and Other Properties of Carbon and Glass Fiber-Reinforced Polymers After Long-Term Weathering in Various Climatic Zones

Elena Vyacheslavovna Dvirnaya[a*], German Victorovich Kornienko[a], Mark Grigorievich Petrov[b], and Oleg Vladimirovich Startsev[a]

[a] *All-Russian Scientific Research Institute of Aviation Materials (NRC « Kurchatov institute»), 17 Radio St., Moscow 105005, Russia*
[b] *Siberian Aeronautical Research Institute named after S.A. Chaplygin, Novosibirsk 630051, Russia*

Abstract In this study, the weathering resistances of glass-fiber-reinforced polymer G1 and two types of carbon-fiber-reinforced polymers, C1 and C2, were studied after six years of outdoor exposure in various climatic zones. Interlaminar shear tests were conducted at strain rates that differed by four orders of magnitude, and dynamic mechanical analyses of these materials were performed both initially and after weathering. Thermal activation analysis of the interlaminar shear test results was used to determine the thermodynamic strength parameter, P_{sh} and durability of the materials. It has been demonstrated that the greatest reduction in the service life of the materials occurs after exposure to the hot and humid climate of Gelendzhik.

Keywords Fiber-reinforced polymers; Weathering; interlaminar shear; Thermal activation analysis; Durability

Citation: Dvirnaya, E. V.; Kornienko, G. V.; Petrov, M. G.; Startsev, O. V. Interlaminar shear strength parameter, durability change and other properties of carbon and glass fiber-reinforced polymers after long-term weathering in various climatic zones. *Chinese J. Polym. Sci.* https://doi.org/10.1007/s10118-026-3648-z

INTRODUCTION

Fiber-reinforced polymers (FRPs) are widely used in the manufacture of aircraft structures.[1,2] Currently, there is an increasing demand for FRP, which can be attributed to its advantages over traditional metal materials. These properties include high strength, rigidity, formability, and excellent corrosion resistance.[3] The requirements for polymer composite materials are stricter than those for metallic materials because of their sensitivity to environmental factors and the variability in their properties. The consistent performance of FRP over extended periods (decades) is crucial to ensure reliability.[4]

Currently, FRP materials based on epoxy-binding polymers are most widely used in aircraft technology.[5,6] However, under the influence of aggressive environmental factors such as extremely high or low temperatures, humidity, solar radiation, and mechanical stress, aging inevitably occurs during exploitation.[7] To investigate the current problem of environmental influence on FRPs, it is necessary to expand the understanding of property degradation processes and compare the roles of various aging factors by exposing the materials to different climatic zones.[8,9] The studies presented in the reviews[10–13] analysed in detail the changes in the basic mechanical properties of various aviation composite materials during weathering at different climatic stations of the Russian Federation.

FRP strength and elastic modulus typically decrease during weathering under natural climatic conditions. For example, Petrova[14] reported that after five years of exposure to the extremely cold climate of Yakutsk, the bending strength (σ_b) of the carbon fiber reinforced polymer (CFRP) based on the adhesive epoxy prepreg KMKU-2m decreased by 9%, and its compressive strength (σ_c) decreased by 10%. It is well known that the corrosive activity of the atmosphere is lower in dry temperate climates compared to humid tropical climates.[15,16] Thus, after 10 years of exposure to EDT-10P binder-based glass fiber-reinforced polymer (GFRP) in a warm, humid climate, the interlaminar shear strength (τ_m) of the surface layers decreased to 55%.[15] Beura *et al.*[17] reported τ_m degradation of epoxy GFRP during weathering in a tropical climate (Jagamara, Odisha, India). After only 60 days of weathering, the deterioration of the properties amounted to 8%. Gavrilieva *et al.*[18] demonstrated the changes in the mechanical properties of epoxy basalt fiber reinforcement bars during weathering in the extremely cold climate of Yakutsk and moderately warm climate of Gelendzhik. After more than 50 months of exposure to Yakutsk, σ_b of basalt fiber reinforcement bars with a nominal diameter of 8 mm decreased by 20%. For a similar Gelendzhik specimen, the decrease in this indicator was 24%. This difference can be at-

* Corresponding author, E-mail: dvirnaya98@mail.ru
Received March 19, 2026; Accepted May 9, 2026; Published online July 1, 2026

tributed to the more humid and warmer climate in Gelendzhik.

Researchers[19] compared the durability performance of GFRP VPS-48/7781 to that of CFRP VKU-39. After one year of exposure in various cities in Russia, including Moscow, Gelendzhik, Sochi, and Yakutsk, σ_c of the materials at 120 °C decreased by 2%–8% for the GFRP and 7%–13% for the CFRP. It is worth noting that in the case of both materials, greater degradation was observed after exposure in the more southern cities of Sochi and Gelendzhik, which have hot and humid climates.[19]

During exploitation, aviation materials are exposed not only to different environments, but also to various mechanical loading conditions, ranging from quasi-static to dynamic loading.[20,21] The FRP temperature sensitivity and strain rate strongly depend on the type of reinforcement and polymer and the performance of the fiber–matrix interfaces.[22,23] Therefore, a fundamental understanding of the effects of test temperature and loading speed on the mechanical behavior of FRP, as well as their interactions, is especially important for the development of composite structures.[24–29] The strain rate and temperature sensitivity can be explained by the transition between different types of molecular mobility.[30–34] For polymer materials, a higher strain rate leads to a shorter relaxation time.[35] In a paper,[36] the authors, using the example of an unreinforced polymer material, revealed the time-temperature superposition principle. This principle describes the equivalence of the time and temperature effects on the strength properties of polymer materials. The study in Ref. [37] describes the mechanical tests of GFRP based on an epoxy matrix. Their study showed that the in-plane shear strength (σ_{12}) was highly dependent on the strain rate. σ_{12} increased from 91 MPa to 137 MPa as the test speed increased from 1×10^{-4} to 6×10^{2} s^{-1}. As reported by Ou *et al.*,[38] the tensile strength (σ_t) of CFRP increased by 36.7% when the loading speed was increased from 25 s^{-1} to 200 s^{-1}. In most similar papers,[39–43] the authors found that the strength of the material was linearly proportional to the logarithm of the strain rate. Nonetheless, the mechanical properties of FRP are complex under different loading speeds and require further research.[44]

In our previous work, we performed an integral analysis of the results obtained from mechanical tests conducted at different strain rates.[45,46] This allowed us to determine the durability of the materials (τ). The loading of a solid material at different temperatures or strain rates causes a change in its activation characteristics during each stage of the failure process because of the molecular mobility of the polymer material.[47,48] Determination of the activation characteristics of a material, such as the initial failure activation energy U_0 (kJ/mol) and activation volume γ (kJ/(mol•MPa)), makes it possible to predict the durability of a material, which depends on the temperature and stress according to the Zhurkov Eq. (1):[47]

$$\tau = t_0 \exp\left(\frac{U_0 - \gamma\tau_m}{RT}\right) \quad (1)$$

where t_0 is the period of thermal oscillation of atoms in a solid (10^{-13} s), R is the universal gas constant (kJ/(mol·K)), T is the test temperature (K), τ_m is the interlaminar shear strength (MPa), τ is the durability of the material or time before failure. This form of the Zhurkov equation is used for interlaminar shear testing.

Eq. (1) is valid only for constant values of the parameters that it includes. In general, when stress, temperature, or structure of a material change, it's necessary to use the rate of failure ($\dot{\omega}$):[45]

$$\dot{\omega} = v_0 \exp\left(-\frac{U_0 - \gamma(t, \tau_i, T)\tau_i(t)}{RT(t)}\right) \quad (2)$$

where v_0 is the characteristic Debye frequency (10^{13} s^{-1}) and the failure rate of destruction is the rate of change in the damage of the material (ω) over time (t) defined as $\dot{\omega} = d\omega/dt$.

The time before the moment of macro-destruction of a material is determined as the integral of the failure rate over time.[45]

$$\int_0^{t^*} \dot{\omega}(t, \tau_i)\, dt = \tau_{eq} v_0 \exp\left(-\frac{U_0 - \gamma\tau_m}{RT}\right) \quad (3)$$

where τ_i is the interlaminar shear stress (MPa) and τ_{eq} is the equivalent failure time or time of the test before failure, s.

Macro-destruction occurs when ω equals 1. The value of ω is inversely proportional to the durability, that is, $\tau = 1/\omega$. Therefore, all the results of the tests at different rates can be analyzed by determining the strength dependence of the fracture activation energy (U). This is known as thermal activation analysis (TAA). If the structure of the material does not change, U is linearly proportional to strength Eq. (4):[45]

$$U(\tau_m) = U_0 - \gamma\tau_m = kT\ln(\tau_{eq}/v_0) \quad (4)$$

The results of the TAA enabled the comparison of the thermodynamic state of a material before and after climatic aging. Previous studies[45] have demonstrated this possibility using an example of CFRP aging in an open environment. This research aims to investigate various indicators, including the activation characteristics of aviation carbon and glass fiber-reinforced polymers based on epoxy matrices before and after long-term outdoor weathering in different climatic zones.

MATERIALS AND METHODS

Materials

GFRP G1 and CFRPs C1 and C2 were chosen as subjects of this study. The main characteristics of these materials are presented in Table 1.[49–52]

All materials were produced at the NRC "Kurchatov Institute" (VIAM) and have been recommended for the manufacture of aircraft structures. The properties of these FRP materials were studied in their initial state and after long-term exposure to various climatic zones.

Outdoor Exposure

CFRP and GFRP plates with dimensions of 300 mm × 300 mm were exposed to outdoor conditions in various climatic zones. In each zone, the specimens were placed on outdoor exposure racks at 45° (horizontal) for 6 years. To study the influence of different climatic factors on the properties of FRPs, we selected the stations listed in Table 2.

3D Scanning Microscopy

To evaluate the surface profiles of the FRP specimens in their initial state and after exposure, 3D scanning microscopy was employed in accordance with ISO 4287:1997. The roughness pa-

Table 1 Main characteristics and mechanical properties of the CFRPs and the GFRP.

Material	Reinforcement	Polymer	Mechanical properties	
			σ_t	σ_c
G1	Satin weave E-glass fiber fabric, areal weight 296 g/m^2 (61%–65 % by weight)	VSE-1212 – DGEBA-based epoxy resin and amine curing agent	450	630
C1	Isotropic carbon reinforcement, areal weight 200 g/m^2 (60%–68 % by weight)	VSE-1212 – DGEBA-based epoxy resin and amine curing agent	945	610
C2	Adhesive prepreg-based carbon reinforcement, areal weight 210–250 g/m^2 60%–62 % by weight)	VSK-14-3 – Chlorine-containing epoxy resin and amine curing agent	1700	1130

Table 2 Climatic stations selected for exposure and their type of climate according to the Köppen classification system.[53,54]

Climate station, city	Material	Classification	Type of climate
Southern Climate Station, Gelendzhik (GCS)	G1 C1 C2	Cfa	Temperate, no dry season, hot summer
Eastern Climate Station, Vladivostok (VCS)	G1 C1 C2	Dwa	Continental, dry winter, hot summer
Northern Climate Station, Dalniye Zelentsy (DCS)	G1 C2	Dfc	Continental, dry winter, cold summer
Western Climate Station, Zvenigorod (ZCS)	G1 C1 C2	Dfb	Continental, no dry season, warm summer
Moscow Climate Station, Moscow (MCS)	G1 C2	Dfb	Continental, no dry season, warm summer

rameters, specifically the maximum height (R_z) and root mean square height (R_q), were measured in representative areas (640 mm × 480 mm) on both the front and back sides of each plate.

Interlaminar Shear Test

The apparent interlaminar shear strength was determined using the short-beam method as specified in ISO 14130:1997. For these tests, specimens were cut from each plate with the dimensions of length × width × thickness = 10h × 5h × h. The specimen thicknesses ranged from 1.8 mm to 3.0 mm. The span (L_s) was set to 5h, and the test specimen was then placed across the two parallel supports. A force was applied across the width of the test specimen. According to the standard, the test speed was 1 mm/min. However, the specificity of our research is precisely a different strain rate, so the speed of the test was in the range of 5×10^{-3}–1×10^{1} mm/min. The maximum values of the tangential stresses were determined using Eq. (5).

$$\tau_m = 3F/4bh \tag{5}$$

where F is the failure or maximum load (N), b and h are the width and thickness of the test specimen (mm), respectively.

Dynamic Mechanical Analysis

The viscoelastic behavior of the matrices G1, C1, and C2 was determined using the dynamic mechanical analysis (DMA) method in a three-point bending mode. Three 50 mm × 10 mm specimens were cut from each plate for analysis. The measurements were carried out in an argon stream with a flow rate of 70 mL/min, at a frequency of 1 Hz, a heating speed of 2 °C/min, and a temperature range of 25–250 °C.

The glass transition temperature (T_g) of the polymer matrix was determined by identifying the peak on the curve of the loss modulus (E'') as a function of the temperature.

Water Uptake Kinetics

To determine the moisture diffusion coefficients (D), two square specimens with each material side length of 80 mm were cut, dried at T=60 °C for 90 days, and then placed in humidity chambers (T=60 °C, RH=95%±5%) also for 90 days. The specimens were weighed using an analytical balance with an accuracy of 10 μg. The average moisture content of the two specimens at time i (w_i) was calculated using Eq. (6):

$$w_i = \frac{(m_0 - m_i)}{m_0} \times 100\% \tag{6}$$

where m_0 is the mass of the specimen in its initial state (g) and m_i is the mass of the specimen at time i, g.

The Fickian diffusion model (7) was used[55] to approximate the experimental data as follows:

$$\begin{aligned} &w(t) = w_0(1 - 8S);\ S = \sum_{i=0}^{N-1} \frac{\exp\left[-n^2 dt\right]}{n^2};\\ &d = D/R^2;\ n = \pi(2i+1);\ i = [0..N-1];\ \frac{1}{R^2} = \frac{2}{L^2} + \frac{1}{H^2} \end{aligned} \tag{7}$$

where t is the duration of moisture conditioning (day), D is the moisture diffusion coefficient (mm^2/day), w_0 is the saturation moisture content (%), and L and H are the length and thickness of the square plate (mm), respectively.

The moisture diffusion coefficients, which represent the rate of moisture uptake, were used to characterize the absorption kinetics of the studied materials.

RESULTS AND DISCUSSION

We conducted a comprehensive study of the influence of different climatic factors on the properties of FRPs. This involves performing a range of tests, including 3D scanning microscopy, interlaminar shear testing at various strain rates, and DMA of the specimens in their initial state and after exposure to five different climatic zones.

To assess the surface conditions of the CFRP and GFRP plates after exposure to various climatic zones, the front surfaces were photographed using a 3D scanning microscope. For example, in Fig. 1, there are 3D surface roughness maps of the front surfaces of the materials in their initial state and af-

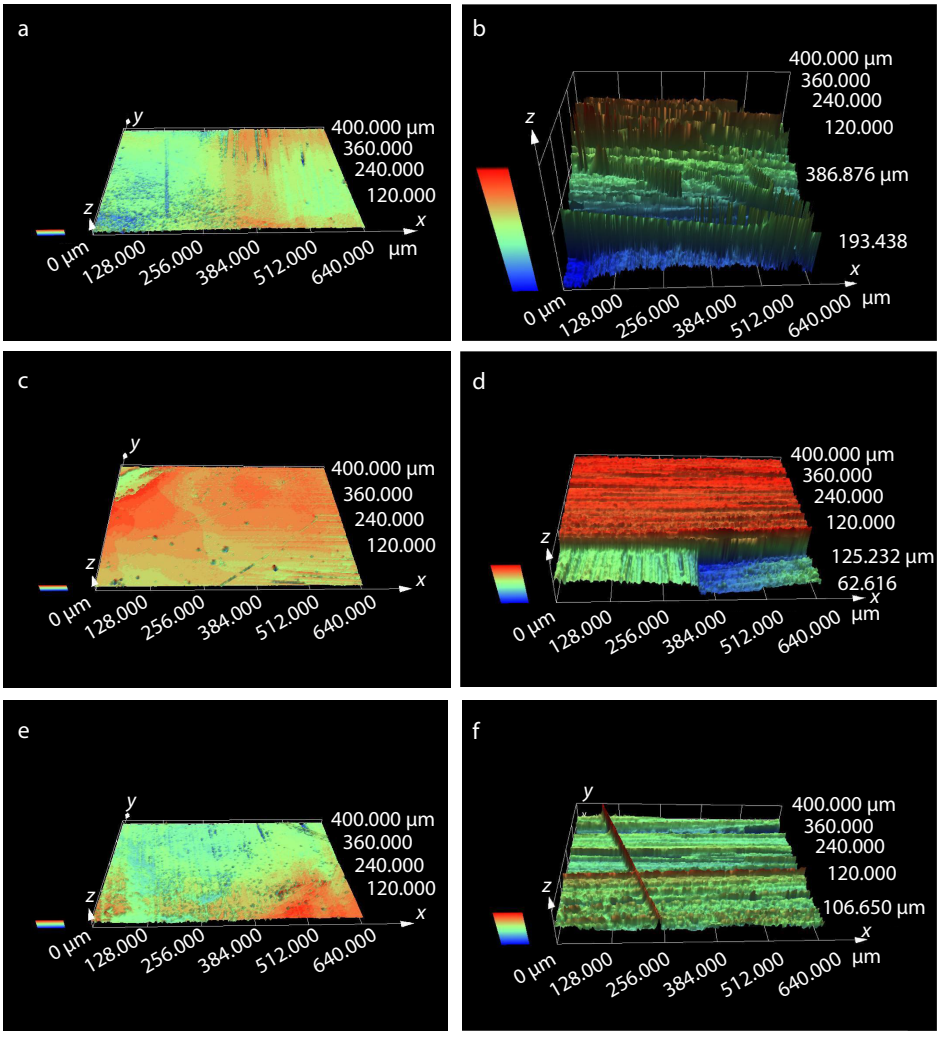

Fig. 1 Microscopy of the front surfaces of FRP plates: (a, b) G1, (c, d) C1 and (e, f) C2 in the initial state (a, c, e) and after 6 years of exposure at the Southern Climate Station (GCS) (b, d, f).

Table 3 the results of the surface profile analysis of the FRP specimens.

Exposure condition	Material	Side	R_z (μm)	R_q (μm)
Initial state	G1	Front	20,2	1,7
		Back	20,8	1,5
	C1	Front	25,4	2,1
		Back	17,2	1,4
	C2	Front	17,3	1,1
		Back	14,3	0,7
After 6 years of exposure at the Southern Climate Station (GCS)	G1	Front	198	22,4
		Back	108	12,4
	C1	Front	100	7,5
		Back	49,6	4,6
	C2	Front	92,3	8,1
		Back	65,2	6,4

ter six years of exposure in Gelendzhik (GCS).

The photographs of the front sides of the FRPs in the initial state (Figs. 1a, 1c, 1e) show the flat-surface layers of the polymer matrices. In Figs. 1(b), 1(d), and 1(f), the fiber is visible as a result of polymer destruction. A similar pattern was typical for all plates after exposure in all climate zones. Table 3 presents the results of the surface profile analysis of the composite FRP materials.

Surface profile analysis of materials G1, C1 and C2 revealed that the RMS height of the front surface elements increased by an order of magnitude following exposure (Table 3). The most significant surface degradation was observed in the G1 specimens.

Under the influence of external climatic factors, the scis-

https://doi.org/10.1007/s10118-026-3648-z

sion of polymer chains occurs in the surface layer of the matrix, leading to embrittlement and deflation of the polymer. The increase in the surface roughness is a direct indicator of matrix degradation, which results in the formation of voids and protruding reinforcing elements. The loss of the protective properties of the outer layer due to degradation can lead to the accelerated destruction of the underlying internal layers. Although the front surfaces degraded most intensely due to direct solar radiation and precipitation, the R_z values for the back surfaces also increased significantly (Table 3). This indicates that certain environmental factors, such as moisture and temperature, can affect the material structure, not only at the exposed surfaces but also throughout the entire bulk of the specimen.

To perform the TAA, the specimens were subjected to interlaminar shear testing at test rates ranging from 5×10^{-3} mm/min to 5×10^{1} mm/min. Fig. 2 shows the dependencies of the interlaminar shear strengths on the loading time in the range of about 5–5000 s for the C1 specimens.

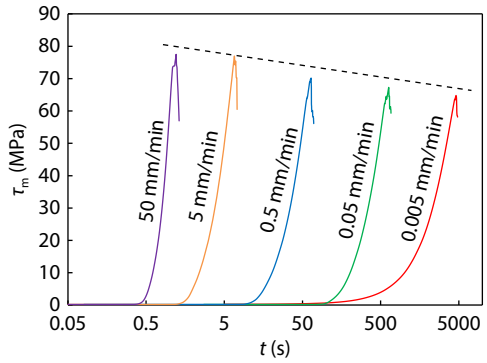

Fig. 2 Dependence of the equivalent failure time on the apparent interlaminar shear strength during testing of CFRP C1.

The strength of the material was linearly proportional to the logarithm of the strain rate. An increase in the strain rate resulted in a shorter relaxation time and an increase in the interlaminar shear strength (Fig. 2).

Then, the results of the tests at different rates were analyzed using TAA. For this purpose, failure rate Eq. (3) was integrated over time steps in accordance with the digitization frequency. As a result, we obtained τ_{eq}, which is the time before τ_m was reached. Then, using the least squares method, the strength dependence $U(\tau_m)$ was calculated with a constant initial activation energy of destruction U_0.

The value of U_0 is closely related to the activation energy of the thermal degradation of a polymer.[47] It is assumed that this indicator is individual for each material and does not depend on structural changes, even after weathering.[45] Despite this, in this study, we determined U_0 for each material after exposure to each zone. For every FRP after weathering at different stations, the values of U_0 are similar. The difference

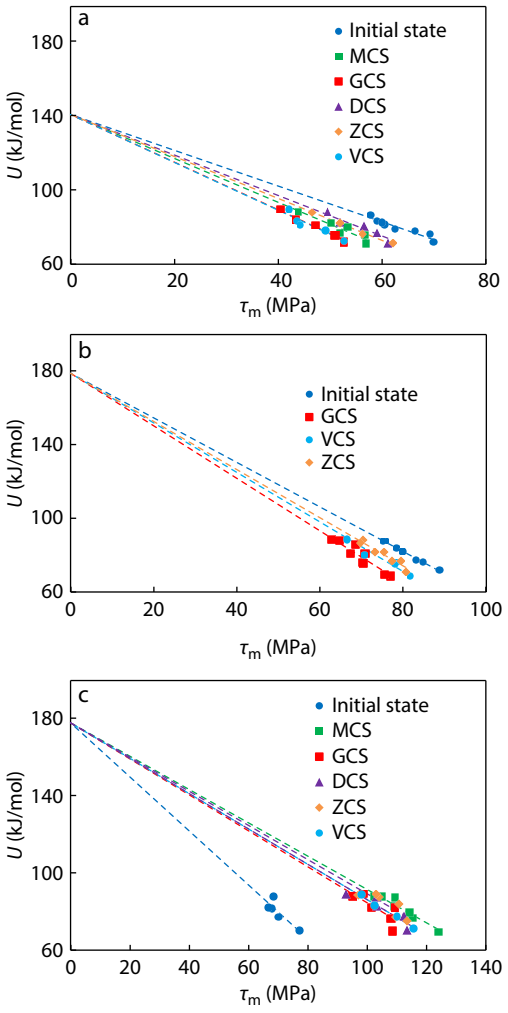

Fig. 3 The FAE dependences on the apparent interlaminar shear strength of G1 (a), C1 (b) and C2 (c) determined by mechanical tests conducted at the different strain rate.

between these values is less than 10%. Therefore, we decided to use the average value of U_0 for all materials after exposure in every zone. Thus, the average values of U_0 for G1, C1, and C2 were 141, 179, and 178 kJ/mol, respectively (Fig. 3). It is important to note that G1 U_0 (Fig. 3a) is similar to that of another GFRP, U_0, which was obtained earlier in Ref. [56].

Conducting tests at strain rates that differ by several magnitudes makes it possible to analyze the area of values that differ by about 15 MPa. To confirm the linear proportionality of the $U(\tau_m)$ dependence, squared deviations from the mean for each material were obtained (Table 4). These statistics demonstrate a strong linear relationship between the fracture activation energies and interlaminar shear strengths.

According to the TAA results, specimens exposed to different climatic zones showed differences in their properties. This

Table 4 The values of squared deviations from the dependences of U_i (kJ/mol) on τ_m (MPa) for the CFRPs and the GFRP, obtained after the TAA.

Material	Initial state	GCS	MCS	DCS	VCS	ZCS
G1	1.42	1.71	2.17	1.76	2.19	0.81
C1	0.48	2.56	–	–	2.50	1.72
C2	3.36	4.40	1.98	3.51	0.94	3.26

https://doi.org/10.1007/s10118-026-3648-z

Table 5 P_{sh}, τ_m and τ for CFRPs and GFRP in the initial state and after weathering in various climatic zones.

Indicator	Initial state	GCS	MCS	DCS	VCS	ZCS
			G1			
P_{sh} ((mol·MPa)/kJ) (k_R)	1.03 (1.00)	0.77 (0.75)	0.84 (0.82)	0.91 (0.88)	0.77 (0.75)	0.88 (0.85)
τ_m (MPa) (k_R)	59.03 (1.00)	43.37 (0.73)	50.12 (0.85)	51.86 (0.88)	43.66 (0.74)	51.91 (0.88)
τ (298 K, 16.45 MPa), year	30	3	7	13	3	10
			C1			
P_{sh} ((mol·MPa)/kJ) (k_R)	0.83 (1.00)	0.70 (0.85)	–	–	0.74 (0.90)	0.76 (0.92)
τ_m (MPa) (k_R)	78.43 (1.00)	67.31 (0.86)	–	–	75.00 (0.96)	73.24 (0.93)
τ (298 K, 44.25 MPa), year	30	1	–	–	3	5
			C2			
P_{sh} ((mol·MPa)/kJ) (k_R)	0.71 (1.00)	1.07 (1.50)	1.16 (1.62)	1.09 (1.53)	1.09 (1.53)	1.13 (1.58)
τ_m (MPa) (k_R)	67.81 (1.00)	101.48 (1.50)	109.29 (1.61)	103.29 (1.52)	102.40 (1.51)	110.84 (1.63)
τ (298 K, 67.21 MPa), year	–	1	4	1	1	2

can be seen in the change in the slope of the regression line for materials from different stations, as quantified by the activation volume (γ) (Fig. 3). This indicator is sensitive to the structural changes in the material. It can change owing to changes in molecular weight or the orientation of polymer chains, or during plasticization and other processes that lead to alterations in the structure of the polymer.[47] The activation volume was calculated using the tangent of the slope $U(\tau_m)$. Then we found (Table 5) the shear strength parameter (P_{sh}) (Eq. 8), which is the inverse of γ. P_{sh} does not depend on the temperature or strain rate during the test but characterizes the state of the material's structure.[45]

$$P_{sh} = \left(\frac{\tau_m}{U_0 - U_i}\right) = \frac{1}{\gamma} \quad (8)$$

In Table 5, the shear strength parameter, P_{sh}, apparent interlaminar shear strength obtained during the test at a strain rate of 0.05 mm/min, τ_m, and durability τ, calculated from Eq. (1) at a temperature of 298 K and a given shear load were also obtained during the test at the same strain rate. In addition, the coefficients of conservation of properties $k_R = (R/R_0)$, where R is P_{sh} and τ_m for the materials after weathering, and R_0 is the indicator for the materials in the initial state (Table 5).

The results obtained during TAA show that P_{sh} is a sensitive indicator that can be used to assess the impact of weathering in different climatic zones. As P_{sh} decreases, τ also decreases under the selected conditions. These conditions (load and temperature) were selected arbitrarily to demonstrate the impact of climatic aging on material durability.

The initial specimens of the G1 and C1 FRPs demonstrated a higher P_{sh} value than the materials after exposure. In the initial state, P_{sh} for VSE-1212 reinforced with glass fiber (G1) was 19% higher than that for the same polymer reinforced with carbon fiber (C1). An opposite trend was observed for the k_R coefficient of these materials after weathering. In all cases, the k_R for CFRP was greater than that for GFRP (by an average of 11%), indicating a lower tendency for degradation of the properties of C1 during weathering. (Fig. 3b) The higher durability values of G1 after exposure can be explained by the lower values of U_0 (Fig. 3a) and given shear load.

Because Eq. (1) accounts only for the effects of the mechanical load and temperature, the durability parameter τ should have remained virtually unchanged after six years of unloaded exposure. The observed reduction in P_{sh}, which led to a decrease in τ by an order of magnitude, was primarily attributed to the contribution of climatic aging and material degradation. The high humidity at the GCS and VCS stations, which can lead to increased ageing, especially during the summer, may cause a significant reduction in the strength parameters of the materials. The irreversible effect of moisture, including the degradation of the polymer matrix due to hydrolysis, is a major contributor to the increased corrosive activity of the atmosphere in coastal areas.[18,57,58] Furthermore, the overheating of the FRP surfaces in the sun during weathering at the GCS may lead to hygrothermal aging processes, resulting in the greatest decrease in P_{sh} for all the materials at this station. For example, the weathering of G1 at the VCS and GCS led to a 26% decrease in P_{sh}.

Despite the similarity between the milder and temperate climates of the MCS and ZCS stations in Moscow, the atmosphere was slightly more polluted. Pollutant agents can also degrade the FRP properties.[59,60] This could explain why the G1 specimens weathered at MCS had a 5% lower P_{sh} than the specimens after exposure to ZCS.

Despite the lower temperature in the northern climate of the DCS, the effect on the strength parameter of weathering at this station was similar to the impact of the temperate climates of the ZCS and MCS. This is because extremely low temperatures have a more negligible effect on the aging of FRPs compared to high temperatures and humidity.[19,61]

The lower P_{sh} value of C2 in the initial state may be due to the post-curing process.[62,63] It is assumed that the strength of the CFRP increased during the first exposure period owing to various factors, and then it decreased at different rates depending on the corrosive activity of different climatic zones. This phenomenon explains the significantly lower durability, τ, of the specimens in their initial states.

The P_{sh} values of C2 specimens after weathering in different climatic zones varied in a smaller range (Fig. 2c) than those obtained for G1 and C1. However, as in the case of G1 and C1 materials, the greatest degradation was observed for C2 specimens after exposure to GCS, while the lowest degradation was observed at stations with a temperate climate (Fig. 3c).

Alterations in moisture transport kinetics are known to sig-

nify structural changes in FRP materials.[64] Consequently, an elevated moisture diffusion coefficient (*D*) indicates damage and degradation after aging. The *D* coefficient is a sensitive marker of physicochemical changes that occur in FRPs during environmental exposure.[65] Fig. 4 shows the value of *D* determined during the moisture uptake test of the investigated FRPs in their initial state and after exposure to different environmental conditions.

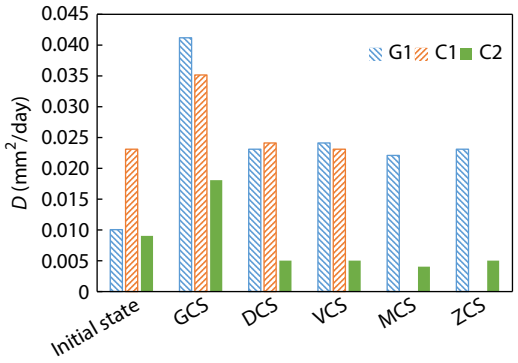

Fig. 4 The values of the moisture diffusion coefficient of the FRPs in the initial state and after 6 years of the exposure.

Consistent with the changes in P_{sh}, the G1 GFRP specimens demonstrated the most significant decrease in moisture saturation resistance after aging. Furthermore, exposure in most climatic zones led to a decrease in the *D* value for C2, which also correlated with the TAA results. At the same time, the highest *D* values for all materials were observed in the samples exposed to GCKI, further confirming the peak atmospheric corrosivity of this station.

Earlier studies of CFRP C1 and GFRP G1 after three years of weathering at these stations showed a slight difference in the properties of materials exposed to different climatic zones.[8,66] The compressive and flexural strengths at two different test temperatures, glass transition temperature of the polymer matrix, and moisture content were chosen as the indicators. The reason for the absence of clear differences could be both the short aging period and high stability of the measured indicators.

We determined the viscoelastic behavior of FRPs polymer matrices after six years of weathering. Table 6 presents the results of dynamic mechanical analysis.

Table 6 The results of DMA testing for CFRP and GFRP materials in the initial state and after weathering in various climatic zones.

Material	Glass transition temperature T_g (°C)					
	Initial state	GCS	MCS	DCS	VCS	ZCS
G1	163.2	154.0	157.4	156.5	155.8	158.6
C1	162.0	169.8	–	–	168.5	169.8
C2	182.0	180.5	182.2	179.4	178.0	178.8

The temperature dependencies of the loss modulus (*E″*) and loss tangent (tanδ) are shown in Fig. 5.

Because C1 and G1 are both made of the same polymer, VSE-1212, the glass transition temperatures of the GFRP and the CFRP in the initial states are almost the same (162–163 °C) (Table 6). However, while the T_g of G1 decreased, the value for

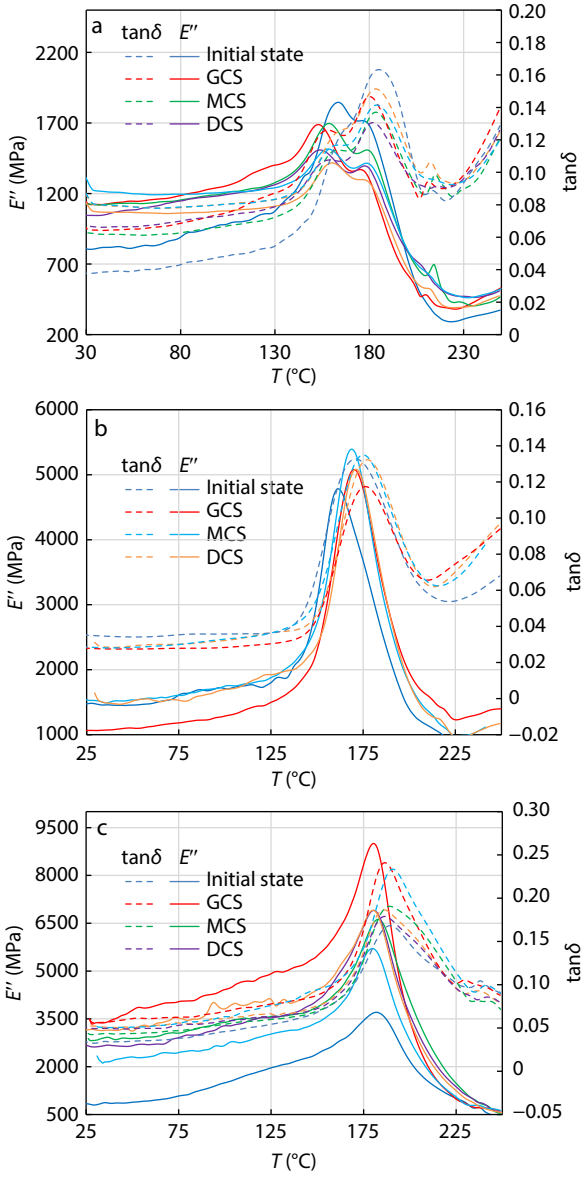

Fig. 5 Dependence of the temperature on the loss modulus and loss tangents for the specimens of G1 (a), C1 (b) and C2 (c) in the initial state and after 6 years of weathering.

C1 increased (Figs. 5a and 5b). The increase in T_g for C1 may indicate matrix post-curing induced by environmental factors, which may result in a transient strength improvement but also render the material more brittle.

As in previous studies of materials after three years of weathering,[8,66] a double peak in the matrix loss modulus of G1 was observed after six years (Fig. 5a). The splitting of the *E″* and tanδ peaks during DMA can be attributed to the superposition of the mechanical and structural relaxation types or the morphological heterogeneity of the initial system. However, Fig. 5(a) reveals that climatic aging led to clearer peak separation, especially in the case of the GCS station. In the case of CFRPs C1 and C2, there were singlet peaks of the maximum loss modulus (Figs. 5b and 5c).

The values of T_g for the C2 CFRP showed a great ability to

https://doi.org/10.1007/s10118-026-3648-z

preserve its properties during weathering (Fig. 5c). The change in the glass transition temperature of the polymer matrix of these materials after six years of exposure in different climatic zones did not exceed 4 °C (Table 6). In the case of G1, which had the lowest ability to maintain viscoelastic properties, there was a precise distribution of T_g over the climatic zones where the material was weathered. Moreover, the glass transition temperatures of the polymer matrices of G1 correlate with P_{sh} of the GFRP after weathering in various climatic zones (Fig. 6).

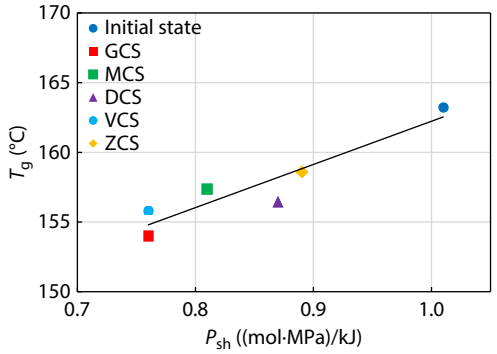

Fig. 6 Dependence of the glass transition temperatures on the shear strength parameter for G1 in the initial state and after 6 years of weathering in various climatic zones.

The high value of the coefficient of determination (0.83) suggests that the durability of a material under shear stress is dependent on its viscoelastic properties.

CONCLUSIONS

Outdoor weathering of three different FRPs was conducted over six years under open conditions at stations in various climatic zones. The thermal activation analysis of the results of the interlaminar shear tests, conducted at different strain rates, allowed us to determine the P_{sh} parameter and durability of the FRPs. The most significant decrease in P_{sh} was observed for materials that had been weathered at the Gelendzhik and Vladivostok climate stations, which are located in coastal areas. Considering the influence of weathering at all climatic stations on the studied FRPs, the GCS, VCS, MCS, ZCS, and DCS stations were in the order of decreasing weathering effect.

In its initial state, polymer VSE-1212 reinforced with glass fiber (G1) demonstrated a higher P_{sh} value than VSE-1212 reinforced with carbon fiber (C1). However, after weathering in all climatic zones, a greater decrease in both the strength parameter and the glass transition temperature was observed for the GFRP than for the CFRP. The studies on the strength properties of FRP materials presented in this paper demonstrate the potential for investigating the thermodynamic processes induced by structural changes in a material during aging. The activation characteristics demonstrated high sensitivity to the effects of different climatic factors on the properties of materials after weathering in various climatic zones.

Conflict of Interests

The authors declare no interest conflict.

Data Availability Statement

The data that support the findings of this study are available from the corresponding author upon reasonable request.

ACKNOWLEDGMENTS

This study was financially supported by the Russian Science Foundation (No. 24-19-00009).

REFERENCES

1 Mahboubizadeh, S.; Sadeq, A.; Arzaqi, Z.; Ashkani, O.; Samadoghli, M. Advancements in fiber-reinforced polymer (FRP) composites: an extensive review. *Discov. Mater.* **2024**, *4*, 22.
2 Parveez, B.; Kittur, M. I.; Badruddin, I. A.; Kamangar, S.; Hussien, M.; Umarfarooq, M. A. Scientific advancements in composite materials for aircraft applications: a review. *Polymers* **2022**, *14*, 5007.
3 Zolkin, A. L.; Galanskiy, S. A.; Kuzmin, A. M. Perspectives for use of composite and polymer materials in aircraft construction. *IOP Conf. Ser.: Mater. Sci. Eng.* **2021**, *1047*, 012023.
4 Soutis, C., in *Polymer Composites in the Aerospace Industry*, ed. by Hayes, P.; Speight, R., Woodhead Publishing, Cambridge, **2015**, pp. 1–18.
5 Kablov, E. N. New generation materials and technologies for their digital processing. *Her. Rus. Acad. Sci.* **2020**, *90*, 225–228.
6 Hasanzadeh, M.; Zadeh, S. M., in *Materials, structures and manufacturing for aircraft*, Springer International Publishing: Cham, **2022**, p. 8.
7 Maraveas, C.; Kyrtopoulos, I. V.; Arvanitis, K. G.; Bartzanas, T. The aging of polymers under electromagnetic radiation. *Polymers* **2024**, *16*, 689.
8 Veligodskiy, I.M.; Koval, T.V.; Kurnosov, A.O.; Marakhovskiy, P. S. study of resistance of glass fiber reinforced plastic to natural weathering in different climatic conditions. *Trudy VIAM* **2022**, *11*, 134–148.
9 Barreira-Pinto, R.; Carneiro, R.; Miranda, M.; Guedes, R. M. Polymer-matrix composites: characterising the impact of environmental factors on their lifetime. *Materials* **2023**, *16*, 3913.
10 Wang, J. U. N.; Gangarao, H. O. T. A.; Liang, R.; Liu, W. Durability and prediction models of fiber-reinforced polymer composites under various environmental conditions: a critical review. *J. Reinf. Plast. Comp.* **2016**, *35*, 179–211.
11 Kablov, E. N.; Startsev, V. O. Climatic aging of aviation polymer composite materials: I. Influence of significant factors. *Russ. Metall.* **2020**, *2020*, 364–372.
12 Lebedev, M. P.; Startsev, O. V.; Kychkin, A. K.; Petrov, M. G.; Kopyrin, M. M. Contributing factors of uneven climatic aging for polymeric composite materials: methods and modelling. *Polymers* **2023**, *15*, 1458.
13 Qin, G.; Fan, Q.; Mi, P.; Li, M.; Mu, W.; Na, J. Review of aging mechanisms, mechanical properties, and prediction models of fiber-reinforced composites in natural environments. *Polym. Compos.* **2024**, *45*, 14448–14474.
14 Petrova, A.P. Properties of adhesives and materials based on them, used under conditions of the arctic. *Review. Klei Germet. Tekhnol.* **2017**, *3*, 38–47.
15 Fang, M.; Zhang, N.; Huang, M.; Lu, B.; Lamnawar, K.; Liu, C.; Shen, C. Effects of hydrothermal aging of carbon fiber reinforced polycarbonate composites on mechanical performance and sand erosion resistance. *Polymers* **2020**, *12*, 2453.
16 Startsev, V. O. Across-the-thickness gradient of the interlaminar shear strength of a CFRP after its long-term exposure to a marine

Graphical Abstract

Interlaminar Shear Strength Parameter, Durability Change and Other Properties of Carbon and Glass Fiber-Reinforced Polymers After Long-Term Weathering in Various Climatic Zones

Elena Vyacheslavovna Dvirnaya, German Victorovich Kornienko, Mark Grigorievich Petrov, and Oleg Vladimirovich Startsev

All-Russian Scientific Research Institute of Aviation Materials (NRC « Kurchatov institute»), Russia; Siberian Aeronautical Research Institute named after S.A. Chaplygin, Russia

This work provides a comprehensive analysis of the degradation mechanisms in three distinct FRP systems exposed to real-world outdoor weathering across five different climatic zones for a period of six years.

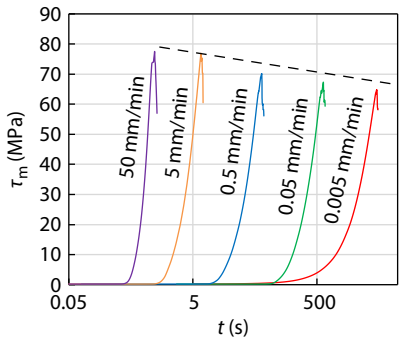

Durability (τ) in accordance with the Zhurkov equation:

$$\tau = t_0 \exp\left(\frac{U_0 - \tau_m \gamma}{RT}\right)$$

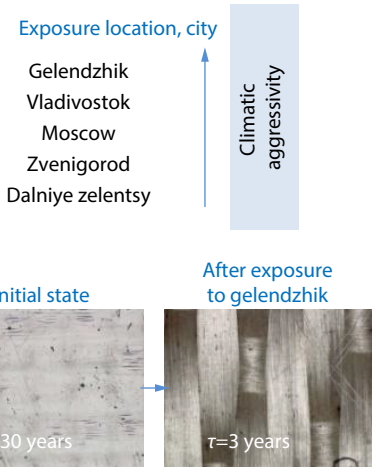

Chinese J. Polym. Sci., 2026 *https://doi.org/10.1007/s10118-026-3648-z*

climate. *Mech. Compos. Mater.* **2016**, *52*, 171–176.
17 Beura, S.; Sahoo, S. R.; Thatoi, D. N.; Mohanty, U. K.; Chakraverty, A. P. Stability of GFRP composites with varied fractions of reinforcement exposed to ageing processes outdoors. *Polym. Compos.* **2021**, *29*, 1485–1494.
18 Gavrilieva, A. A.; Startsev, O. V.; Lebedev, M. P.; Krotov, A. S.; Kychkin, A. K.; Lukachevskaya, I. G. Size effects in climatic aging of epoxy basalt fiber reinforcement bar. *Polymers* **2024**, *16*, 2550.
19 Nikolaev, E. V.; Barbotko, S. L.; Andreeva, N. P.; Pavlov, M. R.; Grashchenkov D.V. A comprehensive study of impacts of climatic and operational factors on a new generation of epoxy binder and polymer composite materials based on epoxy binder. Part 4. Tests of polymer composite materials based on epoxy matrix under natural climatic conditions. *Trudy VIAM* **2016**, *6*, 93–108.
20 Chandra Ray, B.; Rathore, D. A review on mechanical behavior of FRP composites at different loading speeds. *Crit. Rev. Solid State.* **2015**, *40*, 119–135.
21 Mahato, K. K.; Dutta, K.; Ray, B. C. Static and dynamic behavior of fibrous polymeric composite materials at different environmental conditions. *J. Polym. Environ.* **2018**, *26*, 1024–1050.
22 Naser, M. Z.; Hawileh, R. A.; Abdalla, J. A. Fiber-reinforced polymer composites in strengthening reinforced concrete structures: a critical review. *Eng. Struct.* **2019**, *198*, 109542.
23 Ahmed, A.; Rahman, M. Z.; Ou, Y.; Liu, S.; Mobasher, B.; Guo, S.; Zhu, D. A review on the tensile behavior of fiber-reinforced polymer composites under varying strain rates and temperatures. *Constr. Build. Mater.* **2021**, *294*, 123565.
24 Ma, L.; Liu, F.; Liu, D.; Liu, Y. Review of strain rate effects of fiber-reinforced polymer composites. *Polymers* **2021**, *13*, 2839.
25 Zhang, M.; Jiang, B.; Chen, C.; Drummer, D.; Zhai, Z. The effect of temperature and strain rate on the interfacial behavior of glass fiber reinforced polypropylene composites: a molecular dynamics study. *Polymers* **2019**, *11*, 1766.
26 Ou, Y.; Zhu, D. Tensile behavior of glass fiber reinforced composite at different strain rates and temperatures. *Constr. Build. Mater.* **2015**, *96*, 648–656.
27 Cantwell, W. J.; Blyton, M. Influence of loading rate on the interlaminar fracture properties of high-performance composites-a review. *Appl. Mech. Rev.* **1999**, *52*, 199–212.
28 Jacob, G. C.; Starbuck, J. M.; Fellers, J. F.; Simunovic, S.; Boeman, R. G. The effect of loading rate on the fracture toughness of fiber reinforced polymer composites. *J. Appl. Polym. Sci.* **2005**, *96*, 899–904.
29 Thomson, D.; Ploeckl, M.; Hoffmann, J.; Libner, M.; Pohl, C.; Quino, G.; Ramakrishnan, K.; Toenjes, M.; Cui, H.; Petrinic, N. A review of the effect of loading rate on the mechanical properties of unidirectional carbon fibre reinforced polymer composites. *Compos - A: Appl. Sci. Manuf.* **2025**, *193*, 08773.
30 Perry, J. I.; Walley, S. M. Measuring the effect of strain rate on

deformation and damage in fibre-reinforced composites: a review. *J. Dyn. Beh. Mater.* **2022**, *8*, 178–213.
31 Boyce, M. C.; Parks, D. M.; Argon, A. S. Large inelastic deformation of glassy polymers. Part I: rate dependent constitutive model. *Mech. Mater.* **1988**, *7*, 15–33.
32 Adams, D. F.; Adams, L. G. Tensile impact tests of AS4/3501-6 and S2/3501-6 unidirectional composites and the 3501-6 epoxy matrix. *J. Compos. Mater.* **1990**, *24*, 256–268.
33 Gurusideswar, S.; Srinivasan, N.; Velmurugan, R.; Gupta, N. K. Tensile response of epoxy and glass/epoxy composites at low and medium strain rate regimes. *Procedia Eng.* **2017**, *173*, 686–693.
34 Chen, W.; Zhou, B. Constitutive behavior of Epon 828/T-403 at various strain rates. *Mech. Time-depend. Mat.* **1998**, *2*, 103–111.
35 Petrov, M. G. Rheological properties of materials from the point of view of physical kinetics. *J. Appl. Mech. Tech. Phys.* **1998**, *39*, 104–112.
36 Liao, Z.; Yao, X.; Zhang, L.; Hossain, M.; Wang, J.; Zang, S. Temperature and strain rate dependent large tensile deformation and tensile failure behavior of transparent polyurethane at intermediate strain rates. *Int. J. Impact Eng.* **2019**, *129*, 152–167.
37 Tsai, J. L.; Sun, C. T. Strain rate effect on in-plane shear strength of unidirectional polymeric composites. *Compos. Sci. Technol.* **2005**, *65*, 1941–1947.
38 Ou, Y.; Zhu, D.; Zhang, H.; Yao, Y.; Mobasher, B.; Huang, L. Mechanical properties and failure characteristics of CFRP under intermediate strain rates and varying temperatures. *Compos. Part B: Eng.* **2016**, *95*, 123–136.
39 Liu, H.; Pang, Y.; Su, D.; Wang, Y.; Dong, G. A method for plotting failure envelopes of unidirectional polymer composite materials under different strain rates. *Appl. Sci.* **2023**, *13*, 9214.
40 Dumansky, A.; Liu, H.; Alimov, M. Strain-rate effect on mechanical behavior of unidirectional carbon fiber reinforced plastic. *Mater. Today: Proc.* **2019**, *19*, 2377–2381.
41 Xu, X.; Rawat, P.; Shi, Y.; Zhu, D. Tensile mechanical properties of basalt fiber reinforced polymer tendons at low to intermediate strain rates. *Compos. Part B: Eng.* **2019**, *177*, 107442.
42 Reis, J. M. L.; Coelho, J. L. V.; Monteiro, A. H.; da Costa Mattos, H. S. Tensile behavior of glass/epoxy laminates at varying strain rates and temperatures. *Compos. Part B: Eng.* **2012**, *43*, 2041–2046.
43 Zhang, X.; Shi, Y.; Li, Z. X. Experimental study on the tensile behavior of unidirectional and plain weave CFRP laminates under different strain rates. *Compos. Part B: Eng.* **2019**, *164*, 524–536.
44 Khieng, T. K.; Debnath, S.; Ting Chaw Liang, E.; Anwar, M.; Pramanik, A.; Basak, A. K. A review on mechanical properties of natural fibre reinforced polymer composites under various strain rates. *J. Compos. Sci.* **2021**, *5*, 130.
45 Petrov, M. G.; Startsev, O. V.; Lebedev, M. P.; Kopyrin, M. M.; Salnikov, V. G. Strength characteristics of carbon fiber reinforced plastic in shear and cyclic extension-compression after 7 years of climate exposure. *Univers. J. Carbon Res.* **2024**, *2*, 1–13.
46 Petrov, M. G.; Lebedev, M. P.; Startsev, O. V.; Kopyrin, M. M. Effect of Low Temperatures and Moisture on the Strength Performance of Carbon Fiber Reinforced Plastic. *Dokl. Phys. Chem.* **2021**, *500*, 85–91.
47 Regel, V. R. Present state of solid bodies strength physics. *Rheol. Acta.* **1975**, *14*, 19–26.
48 Bartenev, G. M., in *Strength and mechanism of polymer destruction* (In Russian), Khimiya, Moscow, **1984**, p. 34.
49 Raskutin, A. E. Russian polymer composite materials of new generation, their exploitation and implementation in advanced developed constructions. *Aviats. Mater. Tekhn*. **2017**, S, 349–367.
50 Slavin, A. V.; Startsev, O. V. Properties of aircraft glass- and carbonfibers reinforced plastics at the early stage of natural weathering. *Trudy VIAM* **2018**, *9*, 71–82.
51 Kutsevich, K. E.; Dementeva, L. A.; Lukina, N. F. Properties and application of polymer composite materials based on glue prepregs. *Trudy VIAM* **2016**, *8*, 50–57.
52 Marakhovskii, P. S.; Khina, M. B.; Vorob'ev, N. N.; Slavin, A. V. Calculation of the temperature profile during the pressing of a fiberglass based on epoxy resin and a latent hardener. *Russ. J. Gen. Chem.* **2022**, *9*, 1839–1844.
53 Rohli, R. V. in *Atmospheric and Oceanic Circulation*, Springer Nature, Cham, **2024**, p. 249.
54 Lasantha, V.; Oki, T.; Tokuda, D. Data-driven versus Köppen–Geiger systems of climate classification. *Adv. Meteorol.* **2022**, *2022*, 3581299.
55 Crank, J. in *The Mathematics of Diffusion*, 2nd ed., Clarendon press, Oxford, **1975**, p. 414.
56 Petrov, M. G. Analysis of the strength and the durability of an unidirectional GFRP based on the kinetic theory of fracture. *Mech. Compos. Mater. Struct.* **2003**, *9*, 376–397.
57 Startseva, L.; Panin, S.; Startsev, O.; Krotov, A. Moisture diffusion in glass-fiber-reinforced plastics after their climatic aging. *Dokl. Phys. Chem.* **2014**, *456*, 77–81.
58 Ziehl, P.; Anay, R.; Myers, J. J. Durability of fiber-reinforced plastics for infrastructure applications. *Durab. Compos. Syst*. **2020**, 271-288.
59 Zaman, A.; Gutub, S. A.; Wafa, M. A. A review on FRP composites applications and durability concerns in the construction sector. *J. Reinf. Plast. Compos.* **2013**, *32*, 1966–1988.
60 Rosa, I. C.; Castelo, A.; Sousa, J. M.; Garrido, M.; Correia, J. R.; Cabral-Fonseca, S.; de Brito, J. Natural weathering of GFRP structures: case studies, data survey, and proposal of a moisture conversion factor for durability design. *J. Compos. Constr.* **2024**, *28*, 04024063.
61 Startsev, O. V.; Kychkin, A. K.; Lebedev, M. P.; Polyakov, V. V. Effects of moisture on aging of polymer composite materials in a cold climate. *Procedia Struct. Integr.* **2020**, *30*, 162–166.
62 Das, S. C.; La Rosa, A. D.; Goutianos, S.; Grammatikos, S. Effect of accelerated weathering on the performance of natural fibre reinforced recyclable polymer composites and comparison with conventional composites. *Compos. Part C – Open.* **2023**, *12*, 100378.
63 Sousa, J. M.; Correia, J. R.; Cabral-Fonseca, S. Durability of glass fibre reinforced polymer pultruded profiles: comparison between QUV accelerated exposure and natural weathering in a Mediterranean climate *Exp. Tech*. **2016**, *40*, 207–219.
64 Huang, S.; Yan, L.; Kasal, B.; Wei, Y. Moisture diffusion and tensile properties of epoxy-based and polyurethane-based flax-glass hybrid FRP under hygrothermal and weathering environments. Compos. *Part B: Eng.* **2023**, *267*, 111049.
65 Startsev, V. O.; Lebedev, M. P.; Khrulev, K. A.; Molokov, M. V.; Frolov, A. S.; Nizina, T. A. Effect of outdoor exposure on the moisture diffusion and mechanical properties of epoxy polymers. *Polym. Test.* **2018**, *65*, 281–296.
66 Veligodskiy, I. M.; Koval, T. V.; Gulyaev, I. N. Influence of climatic conditions on CFRP VKU-39 after three year outdoor exposition in eight climatic zones *Trudy VIAM* **2023**, *8*, 113–128.